Low Power Consumption Polymer/Silica Hybrid Thermo-Optic Switch Based on Racetrack Resonator

Yuexin Yin, Yue Li, Mengke Yao, Xinyu Lv, Jiaqi Liang, Yuanda Wu, and Daming Zhang

***Abstract*—Large scale integration of photonics devices requires low power consumption devices. In this paper, we demonstrate a low power consumption polymer/silica hybrid thermo-optic switch based on racetrack resonator. With the high index-contrast between SU-8 core, silica buffer and PMMA cladding, a compact racetrack resonator with a small bending radius of 120 μm and a coupling length of 1765 μm is fabricated through simple and low-cost contact lithography technology. An extinction ratio of 16.83 dB is achieved while the power consumption applied is 14.69 mW. The energy efficiency of the switch is 12.07 pm/mW. The rise/fall time the switch is 174 μs/182 μs.**

***Index Terms*—Integrated optics, Optical polymers, Optical resonators, Optical switches.**

I. Introduction

OPTICAL switch, as the key component, has been widely researched and applied on reconfigurable optical add-drop multiplexing (ROADM) and optical cross connection (OXC) systems [1]-[3]. Several optical switches have been demonstrated on different platforms, including silicon-on-insulator (SOI) [4]–[8], silicon nitride (SiN) [9]–[11], silica-based planar lightwave circuits (PLCs) [12]–[16] and polymer-based PLCs [17]–[20]. The low loss waveguide and high coupling efficiency contribute silica-based switch is commercially available and can provide up to 32 ports switching with a fiber-to-fiber loss of 6.6 dB [21]. However, silica switch shows a challenging power consumption for practical integrated electronic circuit cooling technology, owing to the low thermal optical coefficient (TOC) [22]. The silicon photonics (SiPhs), with high refractive index difference and compatible with complementary metal oxide semiconductor (CMOS), are an attractive platform for realizing high density and volume photonics integrated circuits (PICs). Nevertheless, the compact geometry of silicon waveguide leads to high polarization dependence and low coupling efficiency with fiber, which remain challenges for commercialization. Benefitting from large TOC, lower heat conductivity and high-power conversion efficiency, polymer-based PLC technology is an ideal platform for thermo-optic switches. Besides, polymer-based PLC is a potential platform for multifunction integration and have been demonstrated in a variety of applications, including optical network units (ONU) [23]–[25], optical phase arrays (OPA) [26], [27], high speed electro-optic (EO) modulators [28], [29] and optical amplifiers [30], [31]. Among the polymer devices, they are mainly based on straight waveguides or Mach-Zehnder interferometers (MZIs) structure. As a general structure, microring resonators (MRRs) with the key merits of compact size, low power consumption, and wavelength selective function are attractive for high density integration on one chip used for optical interconnects [32], [33], sensing [34], [35] as well as nonlinear applications [36], [37]. However, polymer based MRR switches or tunable filters are less demonstrated. Therefore, in this paper, we demonstrate a low power consumption polymer/silica hybrid thermo-optic switch based on racetrack resonator. To realize a high performance MRR, a straight directional coupler (DC) used in MRR avoids the inter-mode crosstalk. Limited by conventional contact lithography, the gap of 2.5 μm contributes the coupling length to 1765 μm. The MRR is fabricated through simple and low-cost contact lithography. Free spectral range (FSR) of 0.351 nm is obtained with a small 120 μm radius. With voltage applied on the electrode above the ring, a tuning efficiency of 12.07 pm/mW is calculated. The largest extinction ratio 16.83 dB is measured while the power consumption applied is 14.69 mW. A loaded quality factor (Q factor) of 8680 is calculated. Finally, the rise/fall time of the switch is 174 μs/182 μs.

Manuscript received April 5, 2022; revised May 16, 2022; accepted May 29, 2022. Date of publication June 1, 2022; date of current version June 14, 2022. This work was supported in part by the National Key Research and Development Program of China under Grant 2019YFB2203001, and in part by the Science and Technology Development Plan of Jilin Province under Grant 20190302010GX. *(Corresponding author: Daming Zhang.)*

Yuexin Yin, Yue Li, Mengke Yao, Xinyu Lv, Jiaqi Liang, and Daming Zhang are with the State Key Laboratory of Integrated Optoelectronics, College of Electronic Science and Engineering, Jilin University, Changchun 130012, China (e-mail: yxyin20@mails.jlu.edu.cn; liyue19@mails.jlu.edu.cn; yaomk20@mails.jlu.edu.cn; lvxy21@mails.jlu.edu.cn; liangjq21@mails.jlu.edu.cn; zhangdm@jlu.edu.cn).

Yuanda Wu is with the College of Materials Science and Opto-Electronic Technology, University of Chinese Academy of Sciences, Beijing 100049, China (e-mail: wuyuanda@semi.ac.cn).

Digital Object Identifier 10.1109/JPHOT.2022.3179496

II. Structural Design

The polymer/silica hybrid waveguide includes a SiO_2 buffer layer, a SU-8 core and a polymethy-methacrylate (PMMA) cladding as shown in Fig. 1(a). The aluminum (Al) microheater is fabricated above the PMMA cladding. In our design, we choose SU-8 2002 (from Microchem Corporation) as core material. The refractive indices of SiO_2, SU-8 and PMMA are 1.445, 1.573 and 1.483 at 1550 nm, respectively. Compared

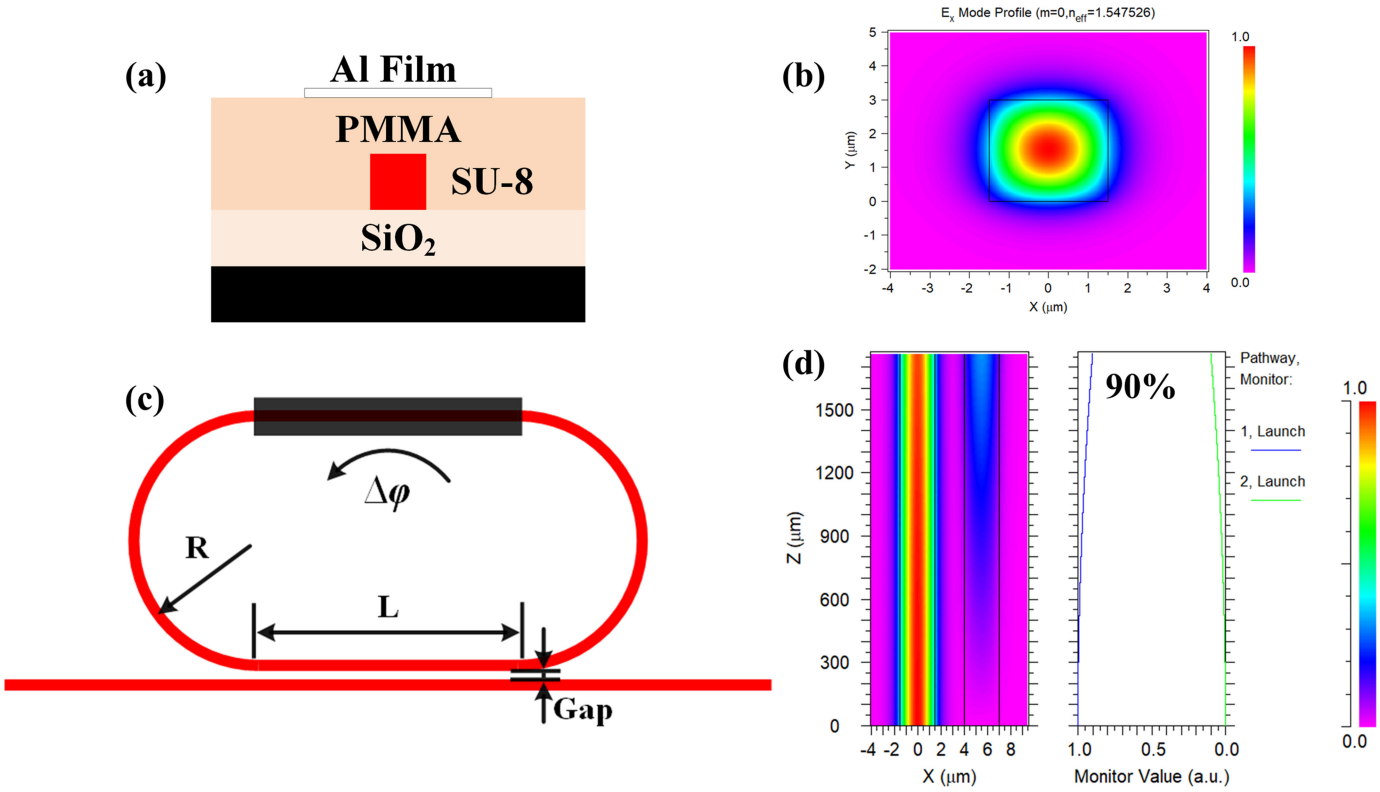

Fig. 1. (a) Cross section of the polymer/silica hybrid waveguide. (b) The TE mode profile of the waveguide simulated through BPM method. (c) Schematic configuration of the present switch based racetrack resonator. (d) Calculated field distribution along the DC at 1550 nm.

with all-polymer devices, silica buffer layer offers an immiscible buffer reducing the solubility phenomenon of waveguide edges after annealing. Besides, a large thermal conductivity (1.4W K^{-1} m^{-1}) of silica boosts the speed. The waveguide dimensions are chosen to be as small as possible, while still be able to produce through conventional contact lithography. Ultimately, the waveguide core dimension is designed to be 3 $\times$ 3 μm^2. The effective refractive index is 1.547-526 for the fundamental transverse electric (TE) mode. The mode profile is shown in Fig. 1(b). The schematic of the switch proposed is shown in Fig 1(c). For a compact footprint, we choose the radius R to be 120 μm. The DC used in the switch avoids inter-mode crosstalk increasing Q factor and extinction ratio (ER) of the device. Limited by ultraviolet (UV) lithography, the gap in DC coupler is chosen to be 2.5 μm. Corresponding to the absorption loss and bend loss, 10% of light is coupled into the racetrack resonator by the DC coupler with the length L of 1765 μm. The field distribution of the optimized DC is shown in Fig. 1(d) at 1550 nm. The same length straight waveguide is tuned by the microheater. With phase change $\Delta\varphi$ introduced, the resonant wavelength is shifted. To improve the coupling efficiency, the width of the input and output waveguides is increased from 3 μm to 16 μm through 200-μm-length tapers.

III. Fabrication and Characterization

In our fabrication, a 15-μm-thick SiO_2 buffer layer was thermally oxidized on a Si substrate. Negative photoresist SU-8 2002 was spin-coated as the core layer onto the silica substrate layer at a rotational speed of 600 r/min and pre-baked with two steps, including 10-min baking at 60 °C. and at 20 mins at 90 °C. Then the coated chip was exposed to ultraviolet (UV) light from a mercury discharge lamp (peak emission wavelength, 365 nm; irradiance, 23 mW/cm^2, ABM-USA, Inc., San Jose, CA, USA) for 4 s and post-baked with two steps, including 10-min baking at 65 °C. and at 20 mins at 95 °C. Time of exposure should be adjusted for a good patter-transfer from the photomask to the SU-8 thin film according to energy density. To remove the unexposed SU-8 polymer, the chip is developed in propyleneglygol-monomethylether-acetate (PGMEA) for 40s, rinsed in isopropyl alcohol followed by de-ionized water. After that, we removed the unexposed SU-8 polymer and then hard-baked it at 120 °C. Finally, a 7-μm-thick PMMA upper cladding was spin-coated on the waveguide cores and baked at 125 °C for 2.5 h. After that, a 500-nm-thick Al film was thermally evaporated over the upper-cladding. Photoresist BP 212 was spin-coated and pattern as a mask above the Al film. The exposed BP 212 and Al were dissolved in a 5‰ NaOH solution. The unexposed BP 212 was removed in an absolute ethyl alcohol solution. A 20-μm-width and 1765-μm-length microheater was formed above the active branch arm. Scanning electron microscope (SEM) images of the switch are shown in Fig. 2. Fig. 2(a) and (b) show cross section of the coupling facet of the switch without/with cladding. Without cladding, the width of coupling waveguide is about 16.336 μm. After PMMA cladding fabrication, the pressure turns rectangular waveguides to trapezoid with slight sidewall

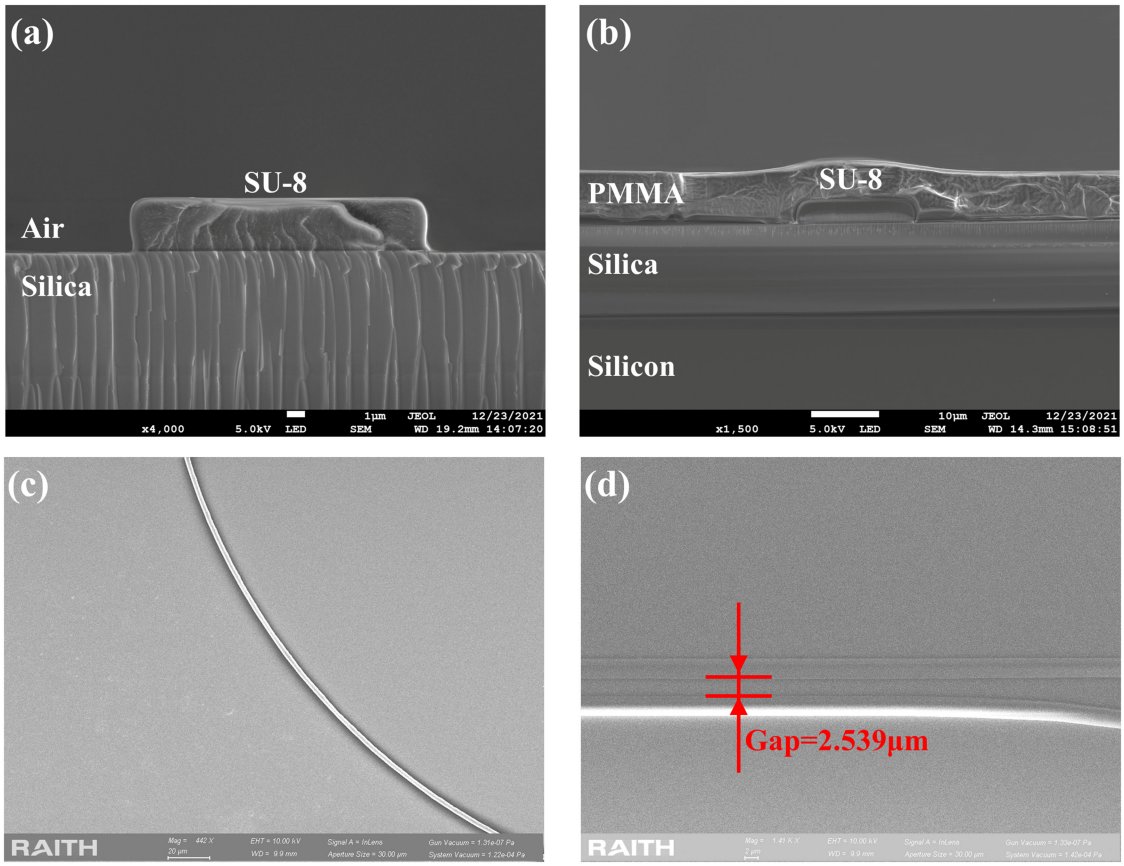

Fig. 2. SEM images of the switch based on racetrack resonator: (a) Cross section of coupling facet without upper cladding. (b) Cross section of coupling facet with upper cladding. (c) Bend waveguide of the switch. (d) DC of the switch.

Fig. 3. Microscope image of the present switch.

angle while the PMMA cladding changing from a liquid to a solid. In Fig. 2(b), the maximum width of the waveguides is about 17.187 μm. The round corner of waveguide caused by PMMA cladding fabrication affects the effective refractive index of waveguide. This unexpected change leads low precision of lithography and excess waveguide loss. Though reactive ion etching (RIE) is an effective method for steep waveguides [[23], [26], [27]], additional mask and dry etching increase the cost and complexity. Another method is filling polymer materials into silica groove. With mature technology of silica-based PLC foundry, this kind of hybrid devices show great potential for commercial applications [[30], [38]]. In Fig. 2(c), the SU-8 switch shows very smooth sidewalls. Fig. 2(d) shows the DC part of the switch, which is agree with the design. The width of waveguides in Fig. 2(c) and (d) is 3 μm.

Fig. 3 shows the microscope image of the present switch with microheater. To characterize the fabricated switch, the fundamental mode from the tunable laser source (TSL-550, Santec, Japan) is launched into the MRR by edge coupling system with a single mode fiber (SMF). The 16-μm-width edge couplers and roughness of the facets increase the coupling polarization dependence. A polarization controller is used for the best coupling. The output power is monitored by an optical power meter (MPM200, Santec, Japan). Owing to narrow linewidth property of MRR, the step size of the tunable laser source is set to be 1 pm.

The resonant wavelength is tuned by applying electric power using source meter instruments (Keithley 2450, Tektronix, Beaverton, OR, USA). Owing to negative thermo-optic coefficient of SU-8, the resonance wavelengths of measured transmission spectra show blue shift as shown in Fig. 4(a). While the refractive index of the waveguide under the microheater changing, the connections between heating and non-heating waveguides lead to excess loss. Therefore, the ER is reducing while applying the voltage. The fiber-to-fiber loss of 17.39 dB includes the propagation loss and coupling loss. The SU-8 waveguide shows a low propagation loss of 2 dB/cm at 1550 nm [39]. The MRR chip is about 2 cm length. Therefore, the coupling loss is about 6.70 dB/facet. The propagation loss mainly results from the material absorption in near infrared wavelengths region and surface scattering. The coupling loss primarily comes from the surface roughness of end facet and fiber-waveguide mode field mismatch. Spot size convertor with adiabatically tapered periodic segmentation [40] is a solution to perform a low loss and polarization independent coupling. From

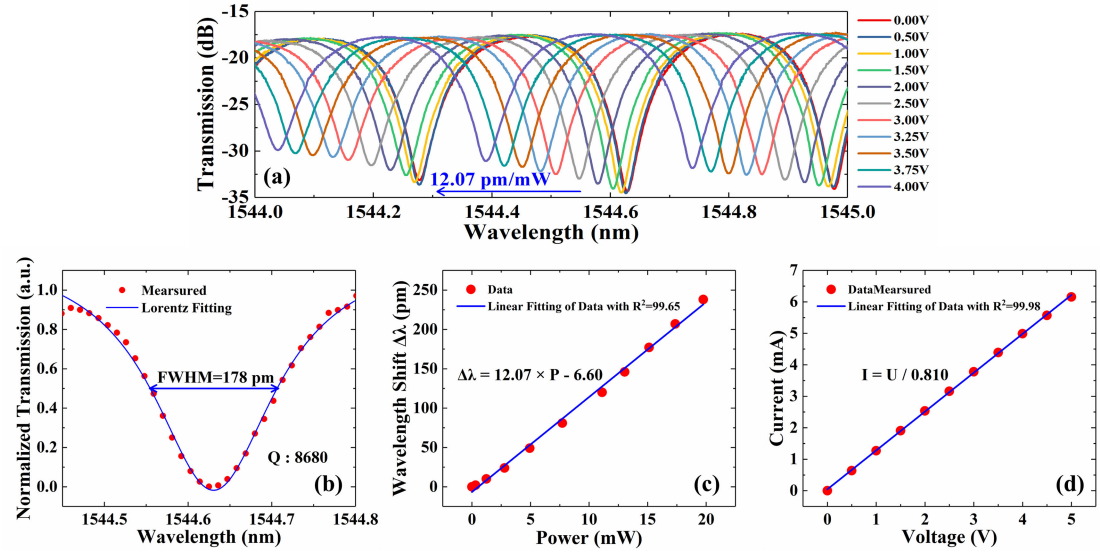

Fig. 4. (a) Transmission spectra of the switch under varying applied voltages. (b) Enlarged view of the measured major resonance peak with Lorentzian Fitting while voltage is 0. (c) Measured Current-Voltage (I-V) curves of the switch. (d) Resonant peak shift of the switch with the heating power.

the measured spectra, the FSR of 0.351 nm and the maximum ER 16.83 dB are obtained. Only the resonance peaks for the fundamental TE mode were observed. Fig. 4(b) is the enlarged view of the major resonance peak. The measured data shown by the red solid circles are fitted well using the theoretical Lorentzian transmission (see the blue solid curve). The full width at half maximum (FWHM) of the resonance peak for the present resonator is about $\Delta\lambda = 178$ pm at 1544.629 nm, which indicates that a loaded Q factor Q_{load} of 8680 is obtained. To characterize the loss in the ring, we calculate the group index $n_g = 1.5859$ from the measured FSR and the path length $L_{tatol} = 2 \times \pi \times R + 2 \times L$ as $n_g = {\lambda_0}^2/(FSR)(L)$. An intrinsic quality factor $Q_{int} \approx 2 \times Q_{load} = 17360$ is obtained at the maximum dip. A propagation loss in ring α_{ring} is 16.17 dB/cm by using equation $Q_{int} \approx 2\pi n_g/\lambda\alpha$ [41]. The loss in ring is larger than the propagation loss of 2 dB/cm. The reason is caused by small radius circular bends and unexcepted fabrication deviation. To overcome these problems, the eular and wider bend is a compact, low loss and fabrication tolerant solution [42], [43].

As shown in Fig. 4(c), linear fitting of the relationship between current and driving voltage applied on 1765-μm-length micro-heater indicates the resistance is 810 Ω. The energy efficiency of the switch is calculated to be 12.07 pm/mW from Fig. 4(d). The energy efficiency can be improved with thinner cladding and air trench.

To measure the switching speed of the device, the MRR is driven by a signal generator (SDG6032X-E, Siglent, China) with two probes. The output light of the MRR is monitored by an oscilloscope (DS4024, RIGOL, China) through a high-speed photodetector. Fig. 5 shows the image of the oscilloscope with both the input driving signal and the output optical signal. The 10%-90% rise and 90%-10% fall time of the switch are 174 μs and 182 μs, respectively, via applying a 3.45 V square-wave driven signal with frequency of 1 kHz and duty cycle of 0.5.

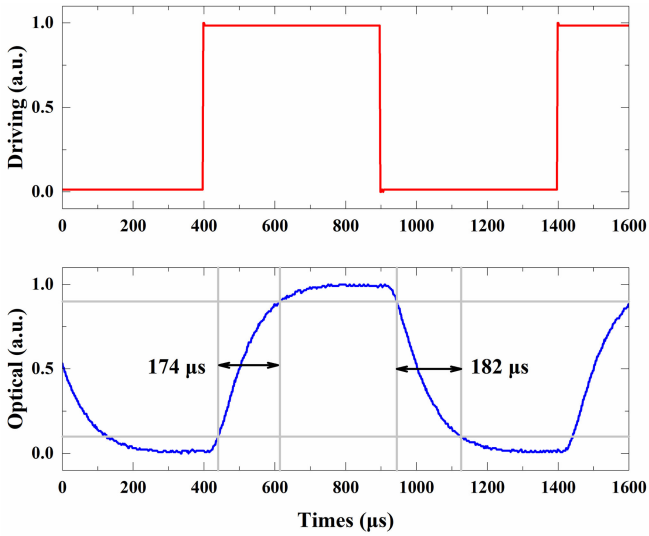

Fig. 5. dynamic response of the fabricated switch.

IV. Discussion

A comparison of MRRs on different platforms reported in recent years is shown in Table I. The resonators are tuned through TO effect in C-band. Owing to high refractive index contrast between the silicon and the silica, compact devices can be realized on a silicon on insulator (SOI) platform. In [44], a 4 $\times$ 4 non-blocking MRR switching is demonstrated on SOI platform. A compact 5-μm-radius ring switch element is tuned by the microheater with a TO efficiency of 250 pm/mW. The TO efficiency has been improved to 1 nm/mW using pulse width modulation (PWM) driver [45]. Another method to conduct TO switch is using front-end of the line (FEOL) heats with doped silicon ridge waveguide. In [46], a cascade MRR filter is tuned

TABLE I
COMPARISON OF MICRORING RESONATORS

Ref.	Platform	ER (dB)	Radius (μm)	Q Factor	Energy Efficiency (pm/mW)
[44]	Silicon on insulator	21	10	~5000	250
[46]	Silicon on insulator	~20	10, 11	9000	2500
[48]	Silicon on insulator	~4	33.9	2×10^4	70
[49]	Silicon on insulator	~4	29	1.3×10^6	N.A.
[50]	Polymer/silica	~18	500	8.2×10^4	2
[51]	Silica on Silicon	13.84	1600	4.47×10^6	4.139
This work	Polymer/silica	16.83	120	8680	12.07

using p-i-p type microheater. The use of vernier effect enlarges the FSR and tuning range. The efficiency of FEOL heats is larger than back-end of the line (BEOL), but the ridge waveguide leads to a large bend. Also, doped regions in the waveguide introduce great nonlinearity [47]. A variety of application can be achieved by integration of MRR with other optical devices. In [48], a MRR array is integrated with an array waveguide grating to conduct an integrated spectrometer. A Q factor of 2×10^4 is obtained with an average radius of 33.9 μm. Thanks to high TOC of silicon, a high energy efficiency of 70 pm/mW is measured. Moreover, to improve the Q factor of SOI resonators, modified Euler curves is introduced. Finally, ultrahigh-Q factor multimode waveguides and multimode waveguide bends with of 1.3×10^6 is achieved [49]. However, the core geometry of 220 nm $\times$ 500 nm contributes polarization dependence and complex coupling method. Besides, compared with polymer-based PLC, fabrication process of SOI devices is expensive and show low tolerances. In [50], a tunable waveguide ring filter is demonstrated with inorganic–organic hybrid optical material named as polysiloxane-liquid series (PSQ-Ls) developed in their group. The homemade materials show a low loss of 0.7 dB/cm at 1550. Therefore, the polymer filter fabricated through UV-soft selective imprint method shows an 8.2×10^4 with a 500-μm-radius. However, nanoimprint lithography (NIL) requires high-cost stamps and high temperatures that might degrade the optical properties of polymer are involved. Therefore, the filter shows a low energy efficiency of 2 pm/mW. In our previous work[51], a high Q factor of 4.47×10^6 is achieved on silica-based PLC. Owing to low TOC of silica, the energy efficiency is 4.139 pm/mW. Low energy efficiency limits large scale integration because of the temperature sensitivity of photonics devices. In this work, the compact racetrack resonator fabricated through simple and low-cost UV lithography and wet etching technology shows a high energy efficiency of 12.07 pm/mW. The maximum ER of 16.83 dB is achieved while the voltage of 3.45 V applied. The power consumption is 14.69 mW. The absorption of SU-8 and small radius lead the Q factor is 8680, which can be improved with the fluorinated SU-8 (FSU-8) [52] and improved fabrication pr–ocess. Multimode waveguides and multimode waveguide bends with modified Euler curves is also an effective method to improve Q factor.

V. CONCLUSION

In summary, we have designed and fabricated a low power consumption thermo-optic racetrack resonator switch based on polymer/silica hybrid waveguide. The compact MRR with a small bending radius of 120 μm and a 1765-μm-length DC coupler is fabricated through simple and low-cost contact lithography. An extinction ratio of 16.83 dB is acquired at 1544.629 nm with 14.69 mW power consumption. The rise and fall time of the switch are 174 μs and 182 μs, respectively. Our measurement results have shown that the fabricated compact racetrack resonator has a Q-factor of 8680. The power consumption can be further depressed by a higher Q resonator through replacing the core material with (FSU-8) and introducing multimode waveguides.

REFERENCES

[1] A. Tsakyridis *et al.*, "Reconfigurable fiber wireless IFoF fronthaul with 60 GHz phased array antenna and silicon photonic ROADM for 5G mmWave C-RANs," *IEEE J. Sel. Areas Commun.*, vol. 39, no. 9, pp. 2816–2826, Sep. 2021.

[2] J. Kundrát *et al.*, "Opening up ROADMs: Streaming telemetry," *J. Opt. Commun. Netw.*, vol. 13, no. 10, pp. E81–E93, Oct. 2021.

[3] K.-I. Sato, "Realization and application of large-scale fast optical circuit switch for data center networking," *J. Lightw. Technol.*, vol. 36, no. 7 pp. 1411–1419, Apr. 2018.

[4] P. Dong, L. Zhang, D. Dai, and Y. Shi, "All-optical switching of silicon nanobeam cavities with an ultra-compact heater utilizing the photothermal effect," *ACS Photon.*, vol. 9, pp. 197–202, 2021.

[5] X. Li, L. Lu, W. Gao, X. Li, J. Chen, and L. Zhou, "Silicon non-blocking 4×4 optical switch with automated polarization adjustment," *Chin. Opt. Lett.*, vol. 19, 2021, Art. no. 101302.

[6] C. Zhong *et al.*, "Fast thermo-optical modulators with doped-silicon heaters operating at 2 μm," *Opt. Exp.*, vol. 29, 2021, pp. 23508–23516.

[7] K. Suzuki *et al.*, "Low-loss, low-crosstalk, and large-scale optical switch based on silicon photonics," *J. Lightw. Technol.*, vol. 38, no. 2 pp. 233–239, Jan. 2020.

[8] Z. Guo, L. Lu, L. Zhou, L. Shen, and J. Chen, "16×16 silicon optical switch based on dual-ring-assisted Mach–Zehnder interferometers," *J. Lightw. Technol.*, vol. 36, no. 2, pp. 225–232, Jan. 2018.

[9] C. Tsokos, *et al.*, "True time delay optical beamforming network based on hybrid InP-silicon nitride integration," *J. Lightw. Technol.*, vol. 39, no. 18, pp. 5845–5854, Sep. 2021.

[10] D. Zheng, J. D. Doménech, W. Pan, X. Zou, L. Yan, and D. Pérez, "Low-loss broadband 5×5 non-blocking Si_3N_4 optical switch matrix," *Opt. Lett.*, vol. 44, 2019, pp. 2629–2632.

[11] J. Joo, J. Park, and G. Kim, "Cost-Effective 2×2 silicon nitride Mach-Zehnder interferometric (MZI) thermo-optic switch," *IEEE Photon. Technol. Lett.*, vol. 30, no. 8, pp. 740–743, Apr. 2018.

[12] Z. Dang *et al.*, "Multiport all-logic optical switch based on thermally altered light paths in a multimode waveguide," *Opt. Lett.*, vol. 46, pp. 3025–3028, 2021.

[13] M.-Z. Ren *et al.*, "Low power consumption 4-channel variable optical attenuator array based on planar lightwave circuit technique," *Chin. Phys. B*, vol. 26, 2017, Art. no. 074221.

[14] M. Takahashi, S. Yamasaki, Y. Uchida, and J. Hasegawa, "Compact and low-loss ZrO_2-SiO_2 PLC-based 8×8 multicast switch for CDC-ROADM application," *J. Lightw. Technol.*, vol. 34, no. 8, pp. 1712–1716, Jun. 2016.

[15] K. Ueda, Y. Mori, H. Hasegawa, K.-I. Sato, and T. Watanabe, "Large-scale optical-switch prototypes utilizing cyclic arrayed-waveguide gratings for datacenters," *J. Lightw. Technol.*, vol. 34, no. 2, pp. 608–617, Jan. 2016.

[16] R. Kasahara, M. Yanagisawa, T. Goh, A. Sugita, A. Himeno, and M. Yasu *et al.*, "New structure of silica-based planar lightwave circuits for low-power thermooptic switch and its application to 8×8 optical matrix switch," *J. Lightw. Technol.*, vol. 20, no. 6, pp. 993–1000, Jun. 2002.

[17] Y. Yuexin *et al.*, "Polymer/silica hybrid waveguide thermo-optic VOA covering O-Band," *Micromachines*, vol. 13, 2022, Art. no. 511.

[18] M. Jiang *et al.*, "On-chip integrated optical switch based on polymer waveguides," *Opt. Mater.*, vol. 97, 2019, Art. no. 109386.

[19] G. He *et al.*, "Low power 1×4 polymer/SiO_2 hybrid waveguide thermo-optic switch," *Opt. Commun.*, vol. 402, pp. 422–429, 2017.

[20] Y. F. Liu *et al.*, "Improved performance of thermal-optic switch using polymer/silica hybrid and air trench waveguide structures," *Opt. Lett.*, vol. 40, pp. 1888–1891, May 2015.

[21] S. Sohma, T. Watanabe, N. Ooba, M. Itoh, T. Shibata, and H. Takahashi, "Silica-based PLC type 32×32 optical matrix switch," in *Proc. Eur. Conf. Opt. Commun.*, 2006, pp. 1–2.

[22] B. G. Lee and N. Dupuis, "Silicon photonic switch fabrics: Technology and architecture," *J. Lightw. Technol.*, vol. 37, no. 1 pp. 6–20, Jan. 2019.

[23] Z. Zhang *et al.*, "Hybrid photonic integration on a polymer platform," *Photonics*, vol. 2, pp. 1005–1026, 2015.

[24] C. Chen *et al.*, "Monolithic multi-functional integration of ROADM modules based on polymer photonic lightwave circuit," *Opt. Exp.*, vol. 22, pp. 10716–10727, May 2014.

[25] C. Chen *et al.*, "Reconfigurable optical interleaver modules with tunable wavelength transfer matrix function using polymer photonics lightwave circuits," *Opt. Exp.*, vol. 22, pp. 19895–19911, Aug. 2014.

[26] A. Raptakis *et al.*, "2D optical phased arrays for laser beam steering based on 3D polymer photonic integrated circuits," *J. Lightw. Technol.*, vol. 39, no. 20, pp. 6509–6523, Oct. 2021.

[27] S. M. Kim, E. S. Lee, K. W. Chun, J. Jin, and M. C. Oh, "Compact solid-state optical phased array beam scanners based on polymeric photonic integrated circuits," *Sci. Rep.*, vol. 11, May 2021, Art. no. 10576.

[28] G. W. Lu *et al.*, "High-temperature-resistant silicon-polymer hybrid modulator operating at up to 200 Gbit s^{-1} for energy-efficient datacentres and harsh-environment applications," *Nature Commun.*, vol. 11, Aug. 2020, Art. no. 4224.

[29] X.-B. Wang *et al.*, "Demonstration of a high-speed electro-optic switch with passive-to-active integrated waveguide based on SU-8 material," *RSC Adv.*, vol. 6, pp. 50166–50172, 2016.

[30] T. Sun *et al.*, "Polymer/silica hybrid waveguide amplifier at 532 nm based on $NaYF_4$:Er^{3+}, Yb^{3+} nanocrystals," *Opt. Lett.*, vol. 46, pp. 5385–5388, Nov. 2021.

[31] M. Zhang *et al.*, "High-gain polymer optical waveguide amplifiers based on core-shell $NaYF_4$/$NaLuF_4$: Yb^{3+}, Er^{3+} NPs-PMMA covalent-linking nanocomposites," *Sci. Rep.*, vol. 6, Nov. 2016, Art. no. 36729.

[32] X. Guo, T. Dai, B. Chen, Y. Wang, H. Yu, and J. Yang, "An ultra-compact 4×4 and 8×8 optical switch based on dual-microring resonators," *IEEE Photon. Technol. Lett.*, vol. 32, no. 21, pp. 1365–1368, Nov. 2020.

[33] Q. Cheng *et al.*, "Ultralow-crosstalk, strictly non-blocking microring-based optical switch," *Photon. Res.*, vol. 7, pp. 155–161, 2019.

[34] X. Tu, S.-L. Chen, C. Song, T. Huang, and L. J. Guo, "Ultrahigh Q polymer microring resonators for biosensing applications," *IEEE Photon. J.*, vol. 11, no. 2, Apr. 2019, Art. no. 4200110.

[35] R. Yang, L. Zhou, H. Zhu, and J. Chen, "Low-voltage high-speed coupling modulation in silicon racetrack ring resonators," *Opt. Exp.*, vol. 23, pp. 28993–29003, Nov. 2015.

[36] Y. Zhang, K. Zhong, and H. K. Tsang, "Raman lasing in multimode silicon racetrack resonators," *Laser Photon. Rev.*, vol. 15, 2020, Art. no. 2000336.

[37] M. Ahmadi, L. Bodiou, W. Shi, and S. LaRochelle, "Comprehensive modeling and design of Raman lasers on SOI for mid-infrared application," *J. Lightw. Technol.*, vol. 38, no. 15, pp. 4114–4123, Aug. 2020.

[38] G. N. Malheiros-Silveira *et al.*, "High-resolution notch filters and diplexers based on SU-8 inverted rib waveguides," *Appl. Opt.*, vol. 58, pp. 7331–7335, Sep. 2019.

[39] C. Changming, Y. Yunji, W. Fei, Y. Yunfei, S. Xiaoqiang, and Z. Daming, "Ultra-long compact optical polymeric array waveguide true-time-delay line devices," *IEEE J. Quantum Electron.*, vol. 46, no. 5, pp. 754–761, May 2010.

[40] M. H. Chou, M. A. Arbore, and M. M. Fejer, "Adiabatically tapered periodic segmentation of channel waveguides for mode-size transformation and fundamental mode excitation," *Opt. Lett.*, vol. 21, pp. 794–796, Jun. 1996.

[41] K. Preston, B. Schmidt, and M. Lipson, "Polysilicon photonic resonators for large-scale 3D integration of optical networks," *Opt. Exp.*, vol. 15, pp. 17283–17290, 2007.

[42] X. Ji *et al.*, "Compact, spatial-mode-interaction-free, ultralow-loss, nonlinear photonic integrated circuits," *Commun. Phys.*, vol. 5, 2022, Art. no. 84.

[43] X. Jiang, H. Wu, and D. Dai, "Low-loss and low-crosstalk multimode waveguide bend on silicon," *Opt. Exp.*, vol. 26, pp. 17680–17689, Jun. 2018.

[44] N. Sherwood-Droz *et al.*, "Optical 4×4 hitless silicon router for optical networks-on-chip (NoC)," *Opt. Exp.*, vol. 16, pp. 15915–15922, Sep. 2008.

[45] M. Bahadori *et al.*, "Thermal rectification of integrated microheaters for microring resonators in silicon photonics platform," *J. Lightw. Technol.*, vol. 36, no. 3, pp. 773–788, Feb. 2018.

[46] Z. Linjie, Z. Xiaoheng, L. Liangjun, and C. Jianping, "Tunable Vernier microring optical filters with *p-i-p* type microheaters," *IEEE Photon. J.*, vol. 5, no. 4, Aug. 2013, Art. no. 6601211.

[47] L. Zhou, H. Zhu, H. Zhang, and J. Chen, "Photoconductive effect on p-i-p micro-heaters integrated in silicon microring resonators," *Opt. Exp.*, vol. 22, pp. 2141–2149, Jan. 2014.

[48] S. Zheng *et al.*, "A single-chip integrated spectrometer via tunable microring resonator array," *IEEE Photon. J.*, vol. 11, no. 5, 2019, Art. no. 6602809.

[49] L. Zhang *et al.*, "Ultrahigh-Q silicon racetrack resonators," *Photon. Res.*, vol. 8, pp. 684–689, 2020.

[50] X. Han *et al.*, "UV-soft imprinted tunable polymer waveguide ring resonator for microwave photonic filtering," *J. Lightw. Technol.*, vol. 32, no. 20, pp. 3924–3932, Oct. 2014.

[51] Y. Yuexin *et al.*, "High-Q-factor tunable silica-based microring resonators," *Photonics*, vol. 8, 2021, Art. no. 256.

[52] Z. Cai *et al.*, "Synthesis and characterization of novel fluorinated polycarbonate negative-type photoresist for optical waveguide," *Polymer*, vol. 61, pp. 140–146, 2015.